ORNL/SPR-2017/436

Light Water Reactor Sustainability Program

IMAC Database v.0.3. – Concrete

Yann Le Pape

August 2017

U.S. Department of Energy
Office of Nuclear Energy

ORNL/SPR-2017/436

Light Water Reactor Sustainability Program
Fusion and Materials for Nuclear Systems Division

IMAC Database v.0.3. – Concrete

ORNL/SPR-2017/436
LWRS-M3LW-17OR0403046

Yann Le Pape

August 2017

Prepared by
OAK RIDGE NATIONAL LABORATORY
P.O. Box 2008
Oak Ridge, Tennessee 37831-6285
managed by
UT-Battelle, LLC
for the
US DEPARTMENT OF ENERGY
Office of Nuclear Energy
under contract DE-AC05-00OR22725

CONTENTS

	Page
LIST OF FIGURES	vi
ACRONYMS	vii
EXECUTIVE SUMMARY	ix
1. CONTEXT	1
2. MOTIVATIONS AND OBJECTIVES	2
3. DEVELOPMENT TOOLS	4
4. CURRENT DEVELOPMENT STATUS	6
4.1 Minerals	6
4.2 Aggregates	6
4.3 Concretes	6
5. UPDATED INTERPRETATION OF THE MINERAL RIVE DATA	8
6. PRELIMINARY INTERPRETATION OF IRRADIATED AGGREGATE DATA	11
6.1 RIVE	11
6.2 Young modulus	15
7. FY2017-18 DEVELOPMENT SCHEDULE	17
8. Acknowledgements	18
APPENDIX	23
A AGGREGATES AND MINERALS HIERACHICAL CLASSIFICATION	23

LIST OF FIGURES

Figures **Page**

1 **(Left)** Scatter plot of experimental and empirical model-based RIVEs of minerals. Red marks: silicates; blue marks: carbonates; green marks: oxides. (●) quartz; (▼) plagioclase; (▲) potassium felspar; (■) pyroxene; (◆) mica; (∗) olivine: [1] forsterite; (►) other silicates; (●) calcite; (▼) dolomite; (◆) siderite; (▲) magnesite; (●) corundum; (▼) hematite; (◆) bromellite; (▲) periclase. (*a*)/(*b*) $\tilde{\varepsilon}^* = \varepsilon^* \pm 0.5\%$. **(Right)** Correlation of the RIVE susceptibility index, $\mathcal{I}$, and the relative maximum volumetric expansion, i.e., normalized by that of quartz, i.e., 17.8%, for different groups of minerals – (hbl) hornblende, (kfs): potassium feldspar, (mic): micas, (ol): olivine (data limited to high-magnesian olivine), (plg): plagioclase, (px): pyroxene, (qz): quartz [Whitney and Evans, 2010]. Vertical dashed lines indicate the uncertainty on the maximum RIVE expansions. Both figures were prepared for a manuscript submitted to the Journal of Nuclear Materials [Le Pape et al., 2017]. x

2 Estimation of post-irradiation cracking of varied aggregates. The theoretical radiation-induced volumetric expansions (RIVEs) are derived from linear homogenization theory applied to uncracked polycrystallin materials (See equations in [Le Pape et al., 2016, Appendix A]). Each mark corresponds to the RIVE of a given aggregate at given fluence and irradiation conditions. The fill color is based of the oxide composition (ternary diagram): Red corresponds to high-silica content, blue to carbonate-rich minerals and, green to other-oxides-rich minerals (typically low-silica content). The size of the mark is proportional to the average grain size. The printed numbers located near each symbol correspond to the aggregate ID# in the IMAC database. Circles around square mark indicates the presence of micas: white for muscovite, black for biotite, or gray if unspecified. xi

3 Risk-assessment of the irradiation effects on concrete and their structural significance. DOE LWRS Strategy. 2

4 Quartz RIVE database: projection in the fluence ($n^{E>10\ keV}.pm^{-2}$)-temperature (°C) plane. Color map of the number of neighboring data (radius: $\delta < 0.15$) from light blue to pink areas indicating low to high density of data. Contour plots indicate iso-number of neighbors. (○): IMAC data. Vertical bars indicate the uncertainties on the irradiation temperature. 8

5 Correlation plot of experimental and empirical model-based RIVEs of minerals. Red marks: silicates; blue marks: carbonates; green marks: oxides. (●) quartz; (▼) plagioclase: albite, oligoclase, labradorite; (▲) potassium felspar: sanidine, microcline; (■) pyroxene: augite, diopside, enstatite; (◆) mica: biotite, muscovite, phlogopite; (∗) olivine: forsterite; (►) other silicates: analcime, nepheline; (●) calcite; (▼) dolomite; (◆) siderite; (▲) magnesite; (●) corundum; (▼) hematite; (◆) bromellite; (▲) periclase. (*a*)/(*b*) $\tilde{\varepsilon}^* = \varepsilon^* \pm 0.5\%$. 10

6 (Left) Ternary diagram of the IMAC database aggregate minerals content in terms of silica, carbonates and other oxides. Each symbol corresponds to one aggregate. Mineral contents are calculated based on their average oxides contents collected in the IMAC mineral database (mostly from [Deer et al., 1963, 1997a,b,c, 2001, 2003, 2004, 2009, 2011]). (Right) Aggregate RIVE database: projection in the fluence ($n^{E>10\ keV}.pm^{-2}$)-temperature (°C) plane (data limited to $T < 230$ °C and $\Phi < 7\ n^{E>10\ keV}.pm^{-2}$to improve the readability of the plot. Color-filled symbol: data recently digitized from [Denisov et al., 2012] (120 data points), the RGB color chart is based on the silica content [SiO_2] (red), the carbonate content [$(Ca, Mg, Fe)CO_3$] (blue) and other oxide content (green). Vertical bars: average irradiation temperature variation. 11

7 Neutron irradiation-induced volumetric expansion of aggregates. Hollow symbols: literature data previously collected in [Field et al., 2015] (114 data points); a similar color chart is adopted: i.e., red for silicates, blue for carbonates and green for 'miscellaneous'. Color-filled symbol: data recently digitized from [Denisov et al., 2012] (120 data points), the RGB color chart is based on the silica content [SiO_2] (red), the carbonate content [$(Ca, Mg, Fe)CO_3$] (blue) and other oxide content (green). †: The neutron energy levels are not always documented in the literature gathered by Field et al. 13
8 Estimation of post-irradiation cracking of varied aggregates. The theoretical RIVEs are derived from linear homogenization theory applied to uncracked polycrystallin materials (See equations in [Le Pape et al., 2016, Appendix A]). Each mark corresponds to the RIVE of a given aggregate at given fluence and irradiation conditions. The fill color is based of the oxide composition (ternary diagram): Red corresponds to high-silica content, blue to carbonate-rich minerals and, green to other-oxides-rich minerals (typically low-silica content). The size of the mark is proportional to the average grain size. The printed numbers located near each symbol correspond to the aggregate ID# in the IMAC database. Circles around square mark indicates the presence of micas: white for muscovite, black for biotite, or gray if unspecified. 14
9 Irradiated aggregates: relative Young modulus as a function of RIVE. Hollow symbols: digitized data from [Denisov et al., 2012, Fig. 3.11] (92 data). Color-filled symbol: reconstructed data from the correlation of [Denisov et al., 2012, Fig. 3.11] and other expansion data [Denisov et al., 2012, Fig. 3.1.-3.4.], the RGB color chart is based on the silica content [SiO_2] (red), the carbonate content [$(Ca, Mg, Fe)CO_3$] (blue) and other oxide content (green). Solid line: exponential decay trend line, $\Delta E/E_0 \approx \exp(-0.528\varepsilon^*)$ with ε^* in (%). ($\triangle$): albitite, gabbro, labradorite, urtite; ($\triangleleft$): auleurolite; ($\diamond$): basalt, diabase; ($\circ$): granite, graniodorite, diorite, andesite; ($\square$): hornblendite; ($\times$): dolomite, limestone; ($\triangleright$): magnesite; ($\triangledown$): pyroxenite, peridotite, olivinite, dunite; ($*$): sandstone; (+): siderite. 16
10 ASTM C294 hierarchical classification of aggregate used in concrete. The ramification extremities show the possible minerals constitutive of the rocks. 24
11 Hierarchical classification of silicates (non exhaustive list). (*) indicates available data obtained by ion-beam irradiation, i.e., critical amorphization dose; (**) corresponds to available data obtained by neutron irradiation. 25

ACRONYMS

ASR	alkali-silica reaction
BASH	Bourne-again shell
CBS	concrete biological shield
dpa	displacement per atom
hcp	hardened cement paste
HLW	high-level waste
ICIC	International Committee on Irradiated Concrete
IMAC	Irradiated Minerals, Aggregates and Concrete
JAMPSS	Japan Aging Management Program for Systems and Structures
KJMA	Kolmogorov-Johnson-Mehl-Avrami
LMA	Levenberg-Marquardt algorithm
LWR	light water reactor
LWRS	Light Water Reactor Sustainability
MD	molecular dynamics
mXRF	micro X-ray fluorescence
OPC	ordinary Portland cement
ORNL	Oak Ridge National Laboratory
QA	quality assurance
RIVE	radiation-induced volumetric expansion
SCM	supplemental cementitious material
TEM	transmission electron microscopy
VCS	version control system
XML	Extensible Markup Language

EXECUTIVE SUMMARY

To develop a more rational classification of irradiation-sensitive aggregates, the LWRS Program has adopted a holistic approach that begins with characterizing irradiated mineral analogues before studying irradiated aggregates. i.e., understanding and modeling the interactions between rock-forming minerals and then addressing irradiated concrete using tools previously developed by the Program.

The development of a concrete materials database is central to this effort and provides an approach to: (1) Connect materials characterization and modeling tools with reliable irradiated properties; (2) Facilitate data searching for correlation analysis; (3) Validate irradiated concrete models, in particular, upscaling models (micro-mechanics or meso-/micro-scale numerical models), i.e, minerals – aggregate – concrete; and, (4) Assess the susceptibility of a specific aggregate or concrete against irradiation. This report, the third of a series of three, provides a summary of the last development progress:

- IMAC v.0.1 – Minerals (December 2016);
- IMAC v.0.2 – Aggregates (April 2017);
- IMAC v.0.3 – Concrete (August 2017);
- IMAC v.1.0 – restricted release (October 2017): Access to a number of beta-users, primarily among the International Committee on Irradiated Concrete (ICIC) members, to this version of the database will be made available. Their feedback will be beneficial to fix potential bugs and errors and continue the data collection work as additional irradiation results are published in the open literature by the Light Water Reactor Sustainability (LWRS) and Japan Aging Management Program for Systems and Structures (JAMPSS) programs in particular.
- IMAC v.1.1 – public release (January 2018): This version of the database will be put on a publicly-accessible server. Access will still require credentials provided by ORNL.

A considerable amount of data were collected from the literature and exported in approximately 100,000 lines of Extensible Markup Language (XML) codes.

The analysis of the minerals database has led to the following results (details included in a manuscript submitted to the Journal of Nuclear Materials):

Figure 1 (Left) The extensive set of neutron-radiation-induced volumetric expansion of rock-forming minerals collected by Denisov et al. [Denisov et al., 2012] ($\approx$ 400 data points) was re-analyzed in order to develop an empirical RIVE model applicable to further research on the effects of irradiation on aggregate and concrete in light water reactors (LWRs). The best regression coefficient, $r^2 \approx 0.95$, was obtained by combining two different modeling techniques: (1) an interpolation-like model based on the relative distance to existing data, and, (2) a non linear regression model assuming varied mathematical forms to describe RIVE as a function of the neutron fluence and the average irradiation temperature. Despite the important uncertainties on the collected data, the proposed model estimates the empirical RIVE within $\varepsilon^* \pm 1.5\%$ with a 90% confidence when the whole dataset is considered.

Figure 1 (Right) The susceptibility to develop an irradiation-induced expansion greatly varies with the nature of minerals. Carbonates, i.e., CO_3^{2-} ion bearing minerals, mainly forming limestones and dolostone, exhibit relatively low RIVEs < 1%. The substitution of Ca by Mg leads to higher RIVEs. Silicates, i.e., $[SiO_4]^{4-}$ bearing minerals show a wide range of maximum RIVE, from a few percents to what appears as the bounding value of 17.8% for quartz. The maximum RIVE of silicate appears to be governed, macroscopically, by three parameters: (a) Primarily, the the dimensionality of SiO_4 polymerization (DOSP), then, (b) the relative number of Si−O bond per unit cell, and, (c) the relative

bonding energy (RBE) of the unit cell. The maximum RIVEs of silicates are ranked in the following decreasing order: quartz, feldspars, pyroxenes and hornblendes. The determination of the maximum RIVE for micas and other tectosilicates , such as nepheline or hornblende, requires additional data. Importantly, the macroscopic RIVE appears, in many cases, to result from internal cracking or "pelletization" of the irradiated minerals, due to impurities or structural heterogeneities (twinnings, perthitic forms, irregular intergrowth forms) possibly causing differential strains.

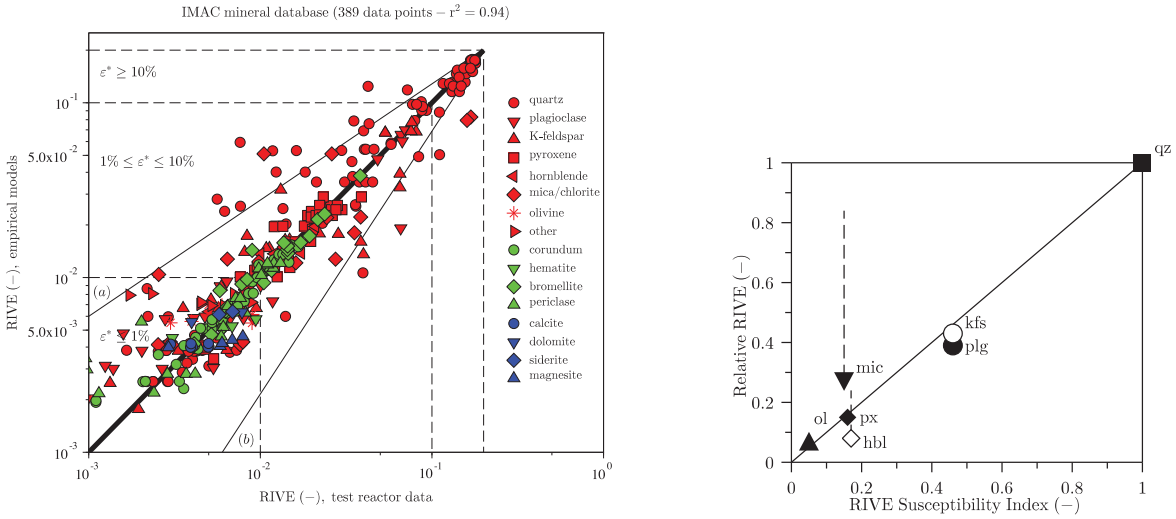

Figure 1. (Left) Scatter plot of experimental and empirical model-based RIVEs of minerals. Red marks: silicates; blue marks: carbonates; green marks: oxides. (●) quartz; (▼) plagioclase; (▲) potassium felspar; (■) pyroxene; (◆) mica; (∗) olivine: [1] forsterite; (►) other silicates; (●) calcite; (▼) dolomite; (◆) siderite; (▲) magnesite; (●) corundum; (▼) hematite; (◆) bromellite; (▲) periclase. (a)**/**(b) $\tilde{\varepsilon}^* = \varepsilon^* \pm 0.5\%$**. (Right) Correlation of the RIVE susceptibility index,** $\mathcal{I}$**, and the relative maximum volumetric expansion, i.e., normalized by that of quartz, i.e., 17.8%, for different groups of minerals – (hbl) hornblende, (kfs): potassium feldspar, (mic): micas, (ol): olivine (data limited to high-magnesian olivine), (plg): plagioclase, (px): pyroxene, (qz): quartz [Whitney and Evans, 2010]. Vertical dashed lines indicate the uncertainty on the maximum RIVE expansions. Both figures were prepared for a manuscript submitted to the Journal of Nuclear Materials [Le Pape et al., 2017].**

The analysis of the aggregates RIVEs database is still in progress. A first approach based on linear homogenization theory applied to uncracked polycrystalline materials (See equations in [Le Pape et al., 2016, Appendix A]) has been developed using mineral composition information and the empirical RIVE models developed previously on the minerals database. The comparison of the RIVE estimates with he experimental data provides a quantification of the extra volumetric change produced primarily by crack formation – Figure 8. Very clearly, high levels of crack formation are observed only in silicate-bearing aggregates. Carbonate-bearing aggregates exhibit low levels of cracking to the exception of a siderite for which the presence of highly expansive quartz (10% in volume fraction) explains the formation of moderate cracking. These findings are found in alignment with previously collected data [Field et al., 2015] and help resolve the ambiguity caused by the general aggregate classification about their tolerance against irradiation: e.g., aggregates designated as *limestones and low-magnesium limestones*, [Kelly et al., 1969] can exhibit large RIVEs after neutron irradiation, very likely caused by the presence of variable amount of silica (possibly

cherts), while nearly pure calcium carbonated rocks, also referred to as *limestone*, exhibit small RIVEs

Other factors, such as the conditions of rock formation, the grain sizes, the differential rock-forming minerals RIVEs, are also currently under investigation as possible factors explaining the cracking development.

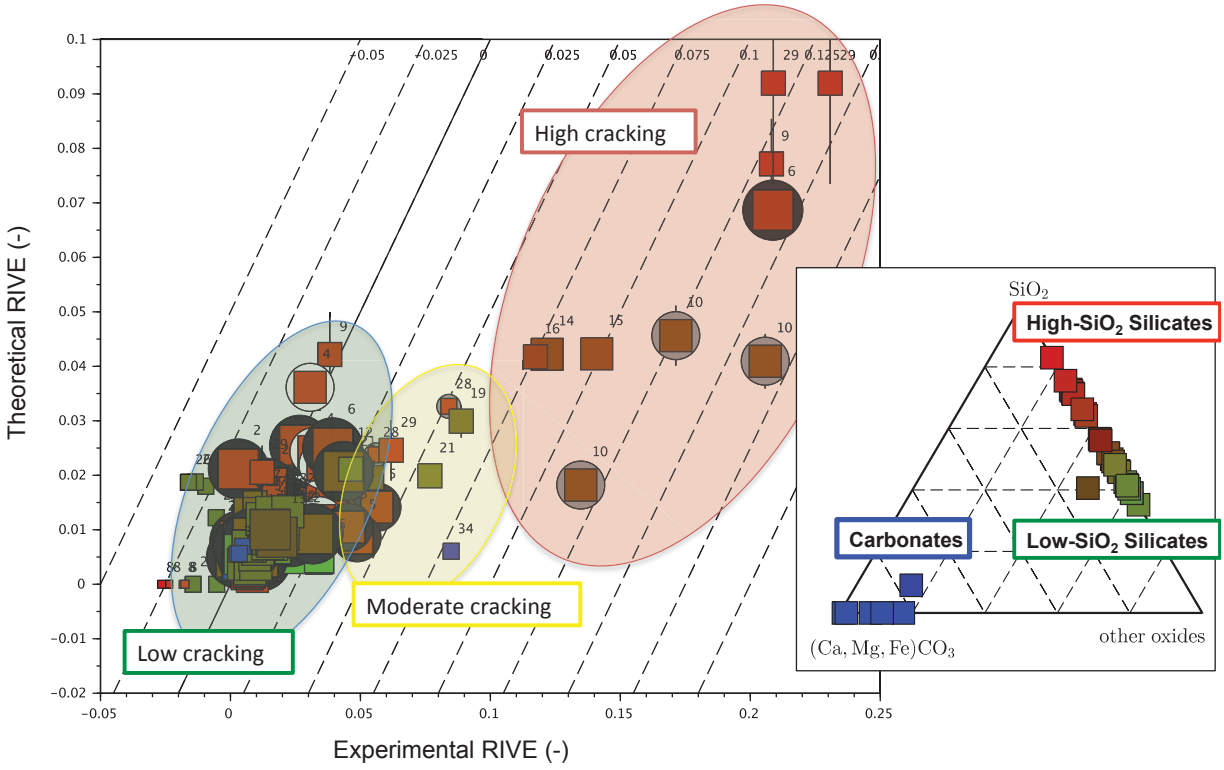

Figure 2. Estimation of post-irradiation cracking of varied aggregates. The theoretical RIVEs are derived from linear homogenization theory applied to uncracked polycrystallin materials (See equations in [Le Pape et al., 2016, Appendix A]). Each mark corresponds to the RIVE of a given aggregate at given fluence and irradiation conditions. The fill color is based of the oxide composition (ternary diagram): Red corresponds to high-silica content, blue to carbonate-rich minerals and, green to other-oxides-rich minerals (typically low-silica content). The size of the mark is proportional to the average grain size. The printed numbers located near each symbol correspond to the aggregate ID# in the IMAC database. Circles around square mark indicates the presence of micas: white for muscovite, black for biotite, or gray if unspecified.

The interpretation of the collected data will continue during FY18 with the objectives of completing two additional reports:

1. The detailed analysis of irradiation-induced aggregate expansion and damage based on IMAC database (December 2017), and,
2. The detailed analysis of irradiation-induced concrete expansion and damage based on IMAC database (April 2018).

1. CONTEXT

Light water reactors (LWRs) concrete biological shields (CBSs) are exposed to high neutrons and gamma irradiations [Fukuya et al., 2002, Esselman and Bruck, 2013, Remec et al., 2016] potentially reaching levels for which degradation has been reported in the literature, i.e., 5×10^{18} n.cm^{-2} at $E > 0.1$ MeV [Hilsdorf et al., 1978, Seeberger and Hilsdorf, 1982]. Reviews of current knowledge on irradiated concrete can be found in [Willam et al., 2013, Rosseel et al., 2016]. At ~80 years of operation, it is estimated that the bounding fluence approaches 6×10^{19} n$^{E>0.1\text{ MeV}}$.cm^{-2}, i.e., about 12 times, the potentially critical dose for irradiation-induce damage onset (As countries other than the U.S. may consider different operation extension periods, the bounding fluence can be estimated proportionally). Susceptibility of concrete to neutron irradiation greatly varies as a function of its constituents, i.e., coarse aggregates, sand, and hardened cement paste (hcp). In particular, higher irradiation-susceptibility was found as a direct function of aggregates RIVE [Elleuch et al., 1972, Field et al., 2015, Le Pape et al., 2015], i.e., the propensity of swelling as a function of their minerals contents, structures and textures. Irradiation-induced amorphization, also referred to as *metamictization* when occurring naturally by α-decay in rocks bearing U, Th…, also induces significant density change, especially in silicates. For example, the maximum volumetric expansion of quartz and feldspars – a group of rock-forming tectosilicate minerals that make up as much as 60% of the Earth's crust [Clarke and Washington, 1924, Wedepohl, 1971] – has been shown to be as large as ≈18% [Primak, 1958, Zubov and Ivanov, 1966] and ≈8% [Krivokoneva, 1976], respectively, while the change of density in calcite remains rather low (≈0.3% according to [Wong, 1974]) Depending on the mineralogical content, considerable variations in aggregate RIVE [Dubrovskii et al., 1967, Kelly et al., 1969, Dubrovskii et al., 1970b, Seeberger and Hilsdorf, 1982] have been observed as described in the comprehensive review by Field et al. [2015]. Moreover, some observed post-irradiation expansions exceed what is considered as detrimental by alkali-silica reaction (ASR) researchers (e.g., [Fournier and Bérubé, 2000, Rajabipour et al., 2015]). Because the CBS structural concrete is made of ≈ 70% of aggregates by volume, RIVE imposes severe stresses on the surrounding hcp leading to micro-cracking, or even fracturing [Le Pape et al., 2015, Giorla et al., 2016]. Because, for obvious economical reasons, the concrete used for the construction of any nuclear power plants structures is made with local materials, large variations of mineralogical composition of aggregate are expected causing major differences in terms of susceptibility against irradiation. Hence, the significance of irradiated structure depends directly on its constituents, and in particular on the aggregate-forming minerals composition, texture and volume fraction.

2. MOTIVATIONS AND OBJECTIVES

The DOE LWRS Program Materials and Aging Degradation Pathway has developed a holistic approach, based on materials characterization and modeling, to assess the susceptibility of concrete against irradiation effects and the structural significance of irradiated concrete biological shield in LWRs. – Figure 3. This approach aims at using experimental data collected in test reactors, and possibly after harvesting from in-service reactor, to help the development and the validation of irradiated concrete models to be utilized for the structural assessment of any specific LWR CBS.

The development of a materials database is central in order to:

1. Connect materials characterization and modeling tools with reliable irradiated properties;
2. Facilitate data searching for correlation analysis;
3. Validate irradiated concrete models, in particular, upscaling models (micromechanics or meso/micro-scale numerical models), i.e, minerals → aggregate → concrete; and,
4. Assess the susceptibility of a specific aggregate or concrete against irradiation.

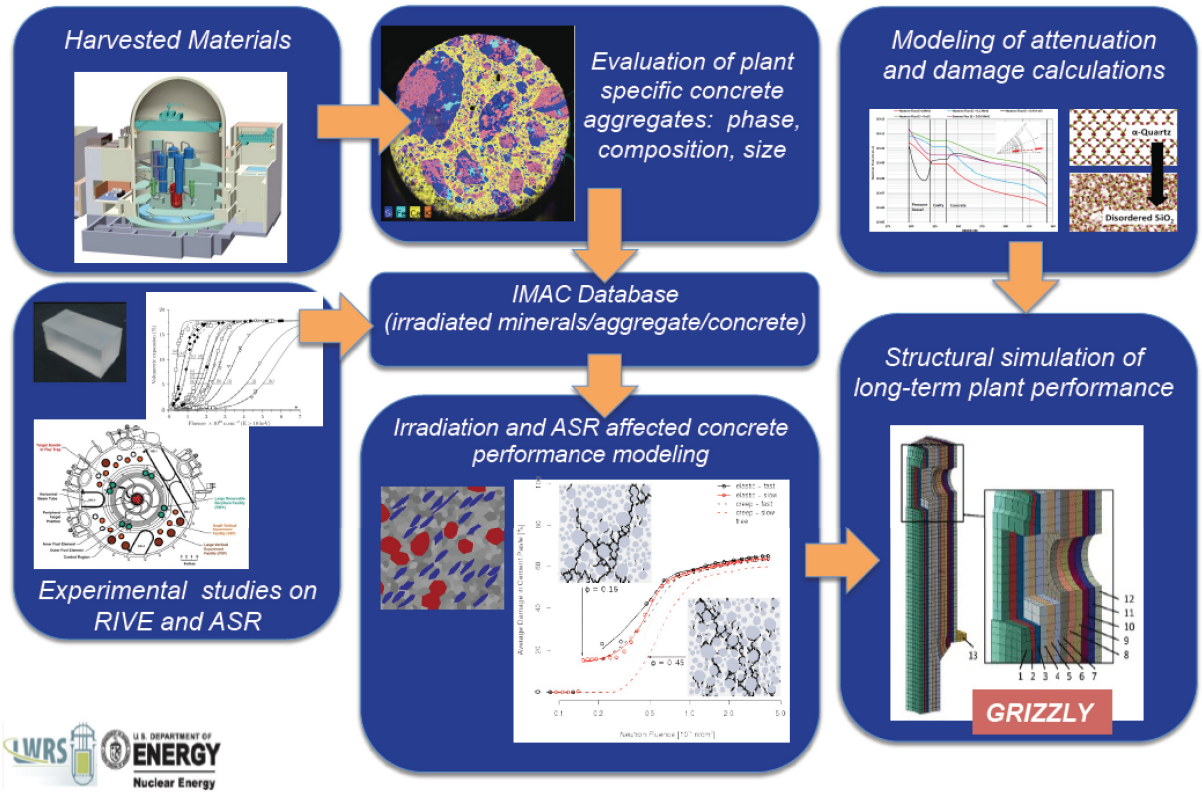

Figure 3. Risk-assessment of the irradiation effects on concrete and their structural significance. DOE LWRS Strategy.

A number of irradiated concrete and aggregate properties (compressive and tensile strength, Young modulus, loss of mass and radiation-induced expansion) have been previously collected [Field et al., 2015]. Although likely-silicate-bearing aggregates were found to be more RIVE-prone than likely-carbonate-bearing aggregates, it appears that the ASTM classification [ASTM C294-12] of aggregates

for concrete fails to define the resistance of aggregates against neutron irradiation. Typical examples can be found in Gray [1971] where different aggregates categorized as *limestone*, i.e, primarily carbonated rocks, exhibit very low expansions, as expected for carbonates, to high linear expansions >1%. The lack of information on the detailed mineralogical contents results in inherent limitations when interpreting the data, in particular, with regard to the large observed scatter. Moreover, the representativity of irradiated aggregate or concrete data against the actual concrete composition used for CBS is more difficult to assess.

Hence, to develop a more rational classification of irradiation-sensitive aggregate, the LWRS Program approach is to adopt a "bottom-to-top" methodology aiming at characterizing irradiated mineral analogues, as a first step, before studying irradiated aggregates. i.e., understanding and modeling the interactions between rock-forming minerals, in a second step, and finally, address irradiated concrete using tools previously developed, e.g., [Le Pape et al., 2015, Giorla et al., 2015, 2017].

Numerous neutron-irradiated minerals RIVE are scattered in the public 'Western' literature, e.g., [Wittels, 1957, Primak, 1958, Wong, 1974, Seeberger and Hilsdorf, 1982]... along with on-going irradiated minerals analogues study at Oak Ridge National Laboratory (ORNL) [Rosseel, 2016]. In addition, more recently, Russian literature was made available to the LWRS Program researchers. These data are extremely valuable as varied minerals, aggregates formed with similar minerals, and concrete made with the same aggregate were tested in similar irradiation conditions. It must also be noted that past research programs related to high-level waste (HLW) storage resulted in the publication of data on the resistance of minerals against ion-irradiation [Eby et al., 1992, Dran et al., 1992]. More recently, electron-irradiation amorphization of minerals was also studied [Muto and Maruyama, 2016]).

However, only limited data on irradiated elastic properties are available: elastic tensor constants, c^*_{ij}, [Mayer and Gigon, 1956, Mayer and Lecomte, 1960, Zubov and Ivanov, 1967] are available for irradiated quartz only. On-going experiments of mineral analogues aims at providing elastic properties for other minerals. It must also be said that molecular dynamics (MD) can help estimate RIVE amplitude and the c^*_{ij} constants of irradiated minerals (in particular, where data is missing), although, some uncertainties about the energy potential in complex crystalline system limit the use of these results.

Finally, the experimental characterization of rock-forming minerals in concrete aggregate using, for example micro X-ray fluorescence (mXRF) and petrographic analysis, requires elements and oxides compositions data.

The Irradiated Minerals, Aggregates and Concrete (IMAC) database aims a collecting all the aforementioned scattered information and data using a systematic approach, including the use of publicly available standard format to export the database and the documentation of the original sources. The database development tools and schedule are provided in sections 3. and 7., respectively.

3. DEVELOPMENT TOOLS

The IMAC database is currently hosted on an internal server at ORNL: `https://code-int.ornl.gov/ylb/IMAC_database`. Access is currently limited to a small number of developers. However, a public release is envisioned for Fall 2017. For the sake of increased quality assurance (QA), the database is being developed and managed by `GitLab`, `https://about.gitlab.com/`, a web-based version control system (VCS) `Git`, `https://git-scm.com/` repository manager with wiki and issue tracking features, using an open source licence. Any committed change, i.e., addition/modification of new/existing data and features, is tracked and recorded. The database uses primarily `Scilab`, `http://www.scilab.org/`, a free open source software for numerical computation, similar to `MatLab`, to:

1. Input and structure data in the database,
2. Export the database in XML files to allow the use of the third-parties software such as finite element code, and,
3. Export the database in LaTeX-format automatically-generated documentation.

The data structures generated in `Scilab` can advantageously be utilized by upscaling micromechanics-type analysis, e.g, [Le Pape et al., 2015]: minerals → aggregate → concrete.

The IMAC repository currently includes the following folders:

`bib` contains the bibliographic database `IMAC.bib`, using BiBTeX reference management software (`http://www.bibtex.org/` – For the sake of convenience, the installation of a graphical application for managing BiBTeX files is recommended: e.g., `JabRef`, `http://www.jabref.org/`, an open software using `Java`). Whenever accessible, copies of the original data sources, i.e., journal articles, proceedings, and sometimes books, are stored in `bib/pdf`. This feature allows future verification of anomalous or suspicious data. Note that BiBTeX citations entries correspond strictly to the cross-reference entries in the database `.sci` files to exchange information between the bibliographic database and the *materials* database

`doc/pub` contains the LaTeX file `IMAC_database.tex` necessary to compile the database in `.pdf` format. Note that `IMAC_database.pdf` being automatically generated, some information can be redundant. For example, each of the < 21 elastic constants data of the minerals includes the information on the experimental technique used (In most cases, the same technique was used to derive all elastic constants of the same mineral). That information is repeated in the exported file. The main reason for these duplications in the `.sci` data files is to ensure that each data point is correctly and thoroughly informed in its data structure to permit efficient data search.

`minerals` contains the minerals database *per se*. Each mineral corresponds to a specific folder name, e.g., `minerals/albite`, containing multiples data files (generally `.sci` files, although some information can also be stored in `.txt` (plain text) files when appropriate, e.g., long tables or figure captions. or `.png` image files, for scanned figure before digitization). For each mineral, a master `Scilab` file loads all information/data. The name of the master file corresponds to the folder name, i.e., the mineral names, e.g., `minerals/albite/albite.sci`.
XML exports also use the mineral names, e.g., `minerals/albite/albite.xml`.
LaTeX exports use the extension `_pub.tex`, e.g., `minerals/albite/albite_pub.tex`.

`aggregates` contains the aggregate database. Aggregates are divided by large categories such as basalt, granite, limestone, to name a few. Each family corresponds to a specific folder name, which contains all corresponding aggregate `Scilab` files.

`concrete` contains the concrete database. Each concrete formulation corresponds to a concrete `Scilab` files. Note that the term *concrete* is here used generically to describe either mortar (low aggregate content, i.e., < 40% in volume fraction) and concrete (high aggregate content, i.e., around 70% volume fraction).

`scilab` contains `Scilab` executable files need to run the database. In particular, loading the database library and exporting the minerals database are performed by launching `quick-screen-minerals.sce` in a `Scilab` console, after configuring and launching `environment_variable.sci` (See `config`).

`config` contains only one configuration file, `environment_variable.sci`, to be edited by each user to provide information about the path to the IMAC database end export options.

`lib` contains all `Scilab` functions library files necessary for description of the data structures, e.g., `mineral_template.sci`, exports, e.g., `xml_export.sci`. It also contains Bourne-again shell (BASH) scripts to extract some general information from publicly-accessible minerals web-database, e.g., `mineral_classification.sh`.

`reactors` contains currently one file only: `list_reactors.sci` linking test reactor names and channels to codes used in the database. Future developments envision to add information on the neutron fluence spectrums.

4. CURRENT DEVELOPMENT STATUS

The August 2017 release includes *minerals*, *aggregates* and *concrete* data.

Currently, the IMAC database contains 44 minerals, 37 aggregates, and >30 different concretes which correspond to about 130 Mb of source code files, `pdf` documentation, and >100,000 lines of XML output data.

4.1 MINERALS

The number of imported mineral may seem poor compared to the >4,500 different known minerals. However, it must be noted that this database is oriented toward concrete aggregate. In that regards, more than 90% on the crust is composed of silicate minerals. Most abundant silicates are feldspars – plagioclase ($approx$40%) and alkali feldspar (≈10%). Other common silicate minerals are quartz (≈10%) pyroxenes (≈10%), amphiboles (≈5%), micas (≈5%), and clay minerals (≈5%) [Wedepohl, 1971]. The rest of the silicate family comprises 3% of the crust. Only 8% of the crust is composed of non-silicates, i.e., carbonates, oxides, sulfides... Although the IMAC database is subject to expansion in the future, the current list of minerals covers, to a large extent, concrete aggregate-forming minerals. Minerals currently available in IMAC are: albite, analcime, andesine, ankerite, anorthite, anorthoclase, augite, biotite, bromellite, bronzite, bytownite, calcite, cassiterite, chamosite, clinochlore, cordierite, corundum, diopside, dolomite, enstatite, fluorapatite, forsterite, hematite, hornblende, hydroxylapatite, labradorite, lizardite, magnesite, magnetite, microcline, muscovite, nepheline, obsidian, oligoclase, orthoclase, periclase, phlogopite, pyrope, quartz, rutile, sanidine, siderite, silica (amorphous), and, spinel. In release v0.2, additional elastic constants data for several unirradiated minerals have been added.

4.2 AGGREGATES

Irradiated aggregate data are currently available for the following rock families (The numbers in parenthesis indicate how many rocks are currently available for each family): albitite (1), aleurolite (1), andesite (1), basalt (1), diabase (3), diorite (1), dolomite (1), dunite (2), gabbro (3), granite (4), granodiorite (2), hematite (1), hornblendite (1), labradorite (1), limestone (3), liparite (1), magnesite (1), obsidian (1), olivinite (1), peridotite (1), pyroxenite (1), sandstone (1), serpentinite (1), siderite (1), and, urtite (1). To the exception of hematite [Dubrovskii et al., 1970a], all data were extracted from Denisov et al. [2012]. Concrete aggregates nature and properties vary as much as the rocks they have been extracted from. Primary factors differentiating rocks are chemical composition (e.g., silicate, carbonate, ore), crystallinity (holocrystalline, cryptocrystalline, hypo-/semi-crystalline, amorphous), texture (size and morphology of grains or crystal, uniformity or heterogeneity), and, formation (magmatic, sedimentary and metamorphic). Available information* of irradiated rocks in Denisov et al. [2012] are: formation, average grain/crystal size, and estimated mineral composition, density, Young modulus, tensile and compressive strength and RIVE. Available information for rocks data collected in Field et al. [2015] usually do not include chemical composition, texture or crystallinity but is limited to generic classification: limestone, basalt...

4.3 CONCRETES

The concrete data have been collected from multiple sources: (1) Western literature data used in Field et al.'s review [Field et al., 2015]; (2) Additional data obtained in Russian test reactors on varied mortars and concretes [Denisov et al., 2012].

*Not fully available for all rocks

The nature and details about the concrete composition and the post-irradiation materials properties vary greatly and inconsistently from one article (or report) to another. When available, the following properties have been reported: compressive strength, tensile strength (indirect measurement from bending test, also formerly known as transverse rupture test [Chisolm Batten, 1960, Fig. 1, p. 399 of.]), Young modulus, loss of weight (induced by drying), and, RIVE. Note that in some instances, the irradiated properties are only provided as relative values against a referenced unirradiated value, not specified. In such case, the property relative value is input in lieu of the absolute value. Note also that the field RIVE can be used as a generic field for volumetric change, i.e., shrinkage of control specimens. Most collected concrete are made of ordinary Portland cement (OPC) although a few are made of aluminous cements[†] (*ciment fondu*), or blended cements, i.e., when a fraction of OPC is substituted by supplemental cementitious materials (SCMs), e.g., fly ash, slag, etc. A large variety of concrete aggregates are reported although limited composition data appears to be available even among the newly-added Russian data. Consequently, future interpretation of the irradiated concrete data will require to account for composition uncertainties when upscaling from the aggregate scale to the concrete scale.

[†]Better performance when exposed to high temperature – Refractory concrete.

5. UPDATED INTERPRETATION OF THE MINERAL RIVE DATA

A thorough analysis of the minerals RIVE currently available in the IMAC database ($\approx<$ 400 data points) has been completed in order to develop empirical models necessary for the interpretation of the aggregate database. The minerals RIVE database can be viewed as a cloud of points in the three-dimensional space of fluence, temperature and volumetric expansion $\left\{\Phi_i, T_i \pm \Delta T_i, \varepsilon_i^*\right\}$. The objective was to develop an empirical model to estimate RIVE as a function of exposure, i.e., $\left\{\tilde{\varepsilon}_i^*\right\} \sim \mathcal{R}(\Phi_i, T_i\})$. Note that in this section, the term *density* indicate the number of data points available in the IMAC database within a given radius in a normalized space of temperature and fluence. Two limitations must be overcome:

1. The data points do not pave consistently the entire Φ-T plane. Figure 4 provides an illustration for quartz, the mineral containing, by far, the highest number of data. Even, in that favorable case, data points form clusters (pink areas) leaving large unchartered portions (light blue areas).

2. The average irradiation temperature is subject to significant uncertainties (vertical 'error' bars in Figure 4).

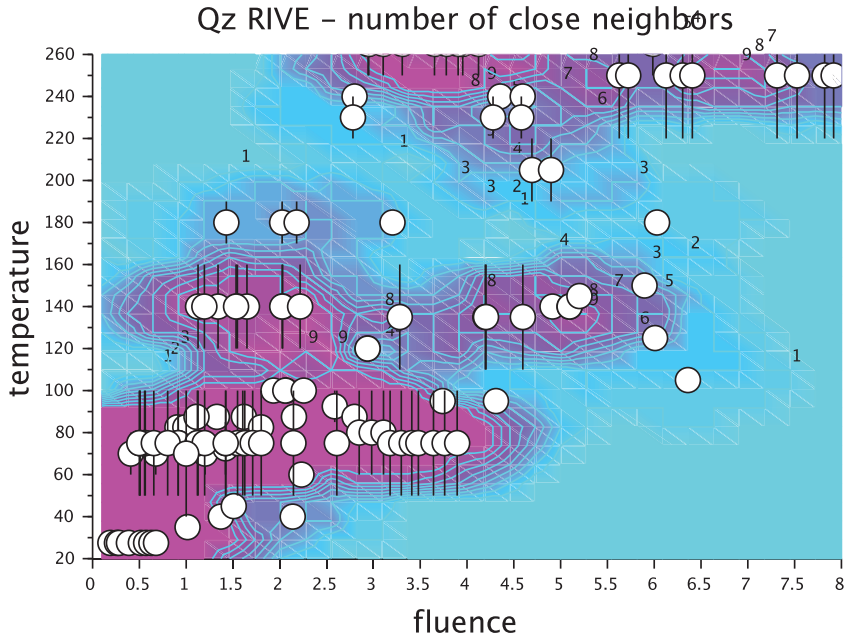

Figure 4. Quartz RIVE database: projection in the fluence ($n^{E>10\ keV}.pm^{-2}$)-temperature (°C) plane. Color map of the number of neighboring data (radius: $\delta < 0.15$) from light blue to pink areas indicating low to high density of data. Contour plots indicate iso-number of neighbors. (○): IMAC data. Vertical bars indicate the uncertainties on the irradiation temperature.

The proposed model is based on a combination of two approaches:

1. A nonlinear regression model, i.e., determination of best-fit parameters, $\{\chi^{(k\leq n)}\}$ (n is the total number of parameters of the model), are derived by nonlinear least squares minimization using Levenberg-Marquardt algorithm (LMA) [Levenberg, 1944, Marquardt, 1963], i.e, finding $\{\chi^k\}$ such as $\min\left(\sum\left(\varepsilon_i^* - \tilde{\varepsilon}_i^*\right)^2\right)$. The adopted RIVE mathematical models vary for each type of minerals, e.g., sigmoidal behavior for most silicates, threshold behavior for carbonates, among others. Note that the

irradiation temperature uncertainties were accounted for by using a probabilistic approach: the average irradiation temperature for each data point is modeled by a uniform distribution $\tilde{T}_i \sim \mathcal{U}(T_i \pm \Delta T_i)$, and, the output best-fit parameters correspond to the average value of 10,000 regression analysis.

2. An interpolation model based on a weighted averaging of the IMAC neighboring data in the areas of sufficient data density.

Both approaches have been tested independently and lead to coefficients of determination, r^2, of ≈ 0.9. The two approaches are combined based on a rule that, in higher data density, the interpolation model is more likely to provide more accurate predictions, while, in lower data density, the nonlinear regression model is likely to be more reliable. The weighting factor is governed linearly by the density of data point in a given radius. Interestingly, the combined model shows an improved coefficients of determination of $r^2 \approx 0.95$ – See Figure 5: Data are plotted using a log-scale for the sake of a better visualization of the complete dataset. Some scatter is still observed at higher expansion levels for some data relative, in particular, to quartz and micas, in particular. The observed scatter for some quartz data is likely to be explained by the uncertainties on the irradiation temperature, and, the likely multiplication of quartz sourcing leading to variation of the tested minerals purity. Micas (phyllo-silicates) are experimentally difficult to work with due to their nearly perfect basal cleavage. In addition, the couple of data on muscovite exhibiting high volumetric expansions > 0.15 at fluence of ≈ 1.5 $n^{E>10\,keV}.pm^{-2}$ were both obtained at the MTR reactor [Crawford and Wittels, 1958], while all other data obtained either in Russian reactors or at Oak Ridge Graphite Reactor show no expansion higher than < 0.05 for fluences up to ≈ 1.25 $n^{E>10\,keV}.pm^{-2}$. Hence, it is difficult to know if this observed 'jump' of RIVE around 1.5 $n^{E>10\,keV}.pm^{-2}$ is caused by abnormal data or by an actual mechanism to be determined. Despite those limitations, the proposed empirical model provides the necessary modeling tools to develop future upscaling modeling of aggregate RIVEs.

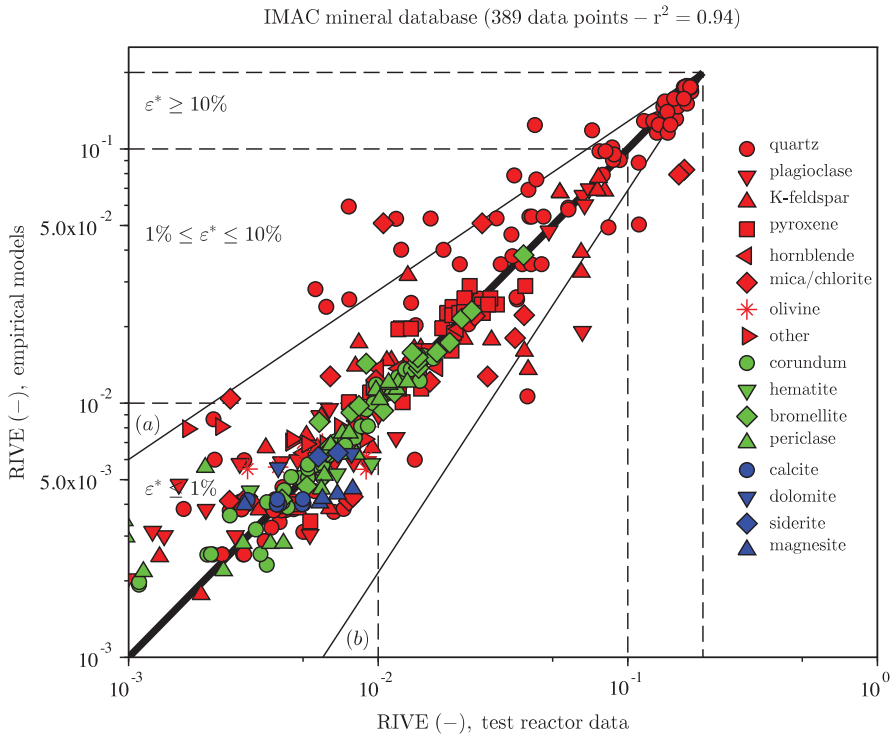

Figure 5. Correlation plot of experimental and empirical model-based RIVEs of minerals. Red marks: silicates; blue marks: carbonates; green marks: oxides. (●) quartz; (▼) plagioclase: albite, oligoclase, labradorite; (▲) potassium felspar: sanidine, microcline; (■) pyroxene: augite, diopside, enstatite; (◆) mica: biotite, muscovite, phlogopite; (∗) olivine: forsterite; (►) other silicates: analcime, nepheline; (●) calcite; (▼) dolomite; (◆) siderite; (▲) magnesite; (●) corundum; (▼) hematite; (◆) bromellite; (▲) periclase. *(a)*/*(b)* $\tilde{\varepsilon}^* = \varepsilon^* \pm 0.5\%$**.**

6. PRELIMINARY INTERPRETATION OF IRRADIATED AGGREGATE DATA

6.1 RIVE

114 aggregate RIVE data points were previously collected by Field et al. [2015] from publicly available literature [Dubrovskii et al., 1970a, Elleuch et al., 1972, Gray, 1971, Kelly et al., 1969, Seeberger and Hilsdorf, 1982]. In addition, Denisov et al. has collected a consistent data set on various aggregates commonly found in concrete, including magmatic and sedimentary rocks, at average irradiation temperatures and neutron fluences ranging, respectively, from 40 °C to 340 °C and 0.1 $n^{E>10\ keV}.pm^{-2}$to 13 $n^{E>10\ keV}.pm^{-2}$ – Figure 6 (Right).

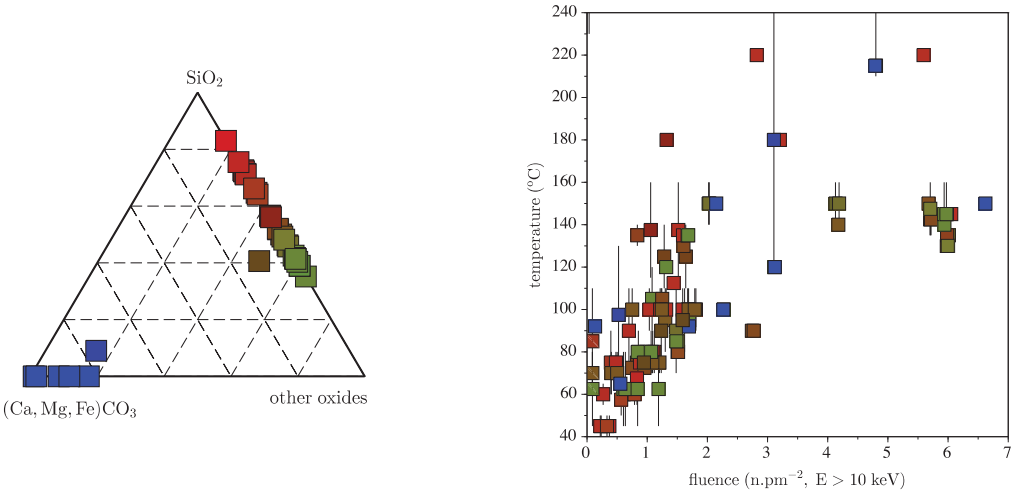

Figure 6. (Left) Ternary diagram of the IMAC database aggregate minerals content in terms of silica, carbonates and other oxides. Each symbol corresponds to one aggregate. Mineral contents are calculated based on their average oxides contents collected in the IMAC mineral database (mostly from [Deer et al., 1963, 1997a,b,c, 2001, 2003, 2004, 2009, 2011]). (Right) Aggregate RIVE database: projection in the fluence ($n^{E>10\ keV}.pm^{-2}$)-temperature (°C) plane (data limited to $T < 230$ °C and $\Phi < 7\ n^{E>10\ keV}.pm^{-2}$to improve the readability of the plot. Color-filled symbol: data recently digitized from [Denisov et al., 2012] (120 data points), the RGB color chart is based on the silica content [SiO_2] (red), the carbonate content [$(Ca, Mg, Fe)CO_3$] (blue) and other oxide content (green). Vertical bars: average irradiation temperature variation.

The principal advantages of Denisov et al.'s data are:

1. All fluence are normalized to an energy threshold of $E > 10$ keV although the data were collected from several testing reactors in Russia. The normalization is based on an equivalent damage principle in terms of displacement per atom (dpa).

2. The mineralogical content (volume fractions) and some indications on the grain size of 34 different aggregates are provided. Figure 6 (Left) shows the ternary diagrams silica-carbonate-other oxides of the concrete aggregate data implemented in the IMAC database: for silicate-based rock, the silica content varies from 0.35 to 0.83, while the carbonates content in carbonated rocks varies from about 0.8 to 1.

Hence, unlike the data set previously assembled by Field et al. [2015], consistency is ensured, and, its appears possible to make a more advanced correlations with the nature of the rock-forming minerals beyond the crude classification: silicates, carbonates and 'miscellaneous'. In particular, future works will include establishing an empirical model for aggregate RIVE explicitly including the mineral composition as a constitutive parameter. Figure 7 shows the RIVE data currently gathered in the IMAC database (114 data points previously gathered by Field et al. [2015] and 120 data points obtained by Denisov et al.'s). From this added dataset, general trends can be observed or confirmed:

1. Carbonated rocks exhibit low expansions. A few exceptions can be noticed and will require further investigation.

2. There appear to be no strict correlation between the amount of silica and expansions at a given fluence (higher silica content corresponds to redder symbol). A possible hypothesis is the importance of differential radiation-induced expansions between aggregate-forming minerals resulting in the formation of cracking at or near grain boundaries.

3. Below $\approx 2\ \mathrm{n}^{\mathrm{E>10\ keV}}.\mathrm{pm}^{-2}$, RIVE rarely exceed 5% to the exception of a specific granite reported by Seeberger and Hilsdorf [1982], i.e., the four data points (red hollow squares) at $< 1 \times 10^{19}$ n.cm^{-2}, thermal neutrons, $E < 1$ eV. Based on the information provided by Seeberger and Hilsdorf, the ratio of fast neutrons ($E > 0.1$ MeV) to thermal neutrons ($E < 1$ eV) equals 5% for the research reactor FR2 at KFZ Karlsruhe. Hence, the actual corresponding fluence at $E > 10$ keV (Denisov et al.'s normalizing fluence) for Seeberger and Hilsdorf's data would be shifted even further toward lower values. Interestingly, the same author also studied other rocks, including quartzite (92% silica content), i.e., quartz grains cemented by silica, the most RIVE-prone silicates, that exhibit expansions, at least, one order of magnitude lower than the studied granite. In terms of expansion amplitudes, those data appears consistent, or at least, not abnormal, with the other aggregates collected in the IMAC database. Other irradiated granites data collected by Denisov et al. do not show early-stage high expansions. While there is no valid reason to exclude Seeberger's granite data from the whole dataset, this early-stage irradiation-induced swelling, leading ultimately to the *destruction* of the Schwarzwald granite raises the question of the driving mechanism specifically involved in this particular behavior. Further research is needed in that direction.

The analysis of the aggregates RIVEs database is still in progress. A first approach based on linear homogenization theory applied to uncracked polycrystallin materials (See equations in [Le Pape et al., 2016, Appendix A]) has been developed using mineral composition information and the empirical RIVE models developed previously on the minerals database. The comparison of the RIVE estimates with he experimental data provides a quantification of the extra volumetric change produced primarily by crack formation – Figure 8. Very clearly, high levels of crack formation are observed only in silicate-bearing aggregates. Carbonate-bearing aggregates exhibit low levels of cracking to the exception of a siderite for which the presence of highly expansive quartz (10% in volume fraction) explains the formation of moderate cracking. These findings are found in alignment with previously collected data [Field et al., 2015] and help resolve the ambiguity caused by the general aggregate classification about their tolerance against irradiation: e.g., aggregates designated as *limestones and low-magnesium limestones*, [Kelly et al., 1969] can exhibit large RIVEs after neutron irradiation, very likely caused by the presence of variable amount of silica (possibly cherts), while nearly pure calcium carbonated rocks, also referred to as *limestone*, exhibit small RIVEs

Other factors, such as the conditions of rock formation, the grain sizes, the differential rock-forming minerals RIVEs, are also currently under investigation as possible factors explaining the cracking development.

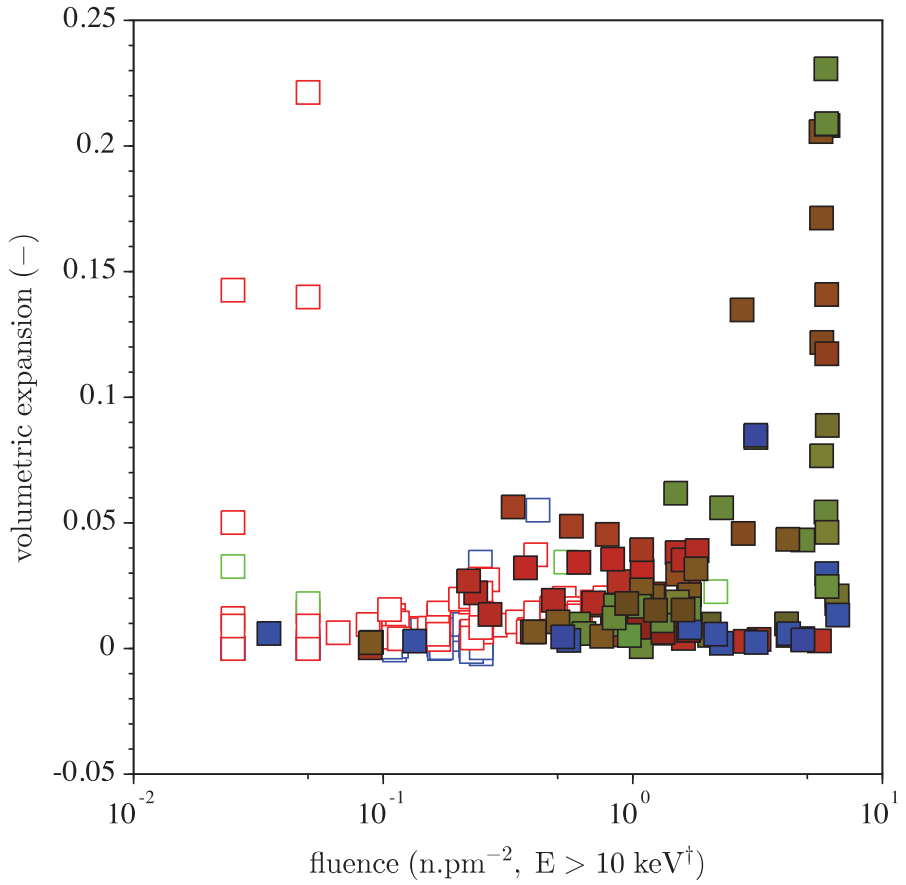

Figure 7. Neutron irradiation-induced volumetric expansion of aggregates. Hollow symbols: literature data previously collected in [Field et al., 2015] (114 data points); a similar color chart is adopted: i.e., red for silicates, blue for carbonates and green for 'miscellaneous'. Color-filled symbol: data recently digitized from [Denisov et al., 2012] (120 data points), the RGB color chart is based on the silica content [SiO_2] (red), the carbonate content [$(Ca, Mg, Fe)CO_3$] (blue) and other oxide content (green). †: The neutron energy levels are not always documented in the literature gathered by Field et al.

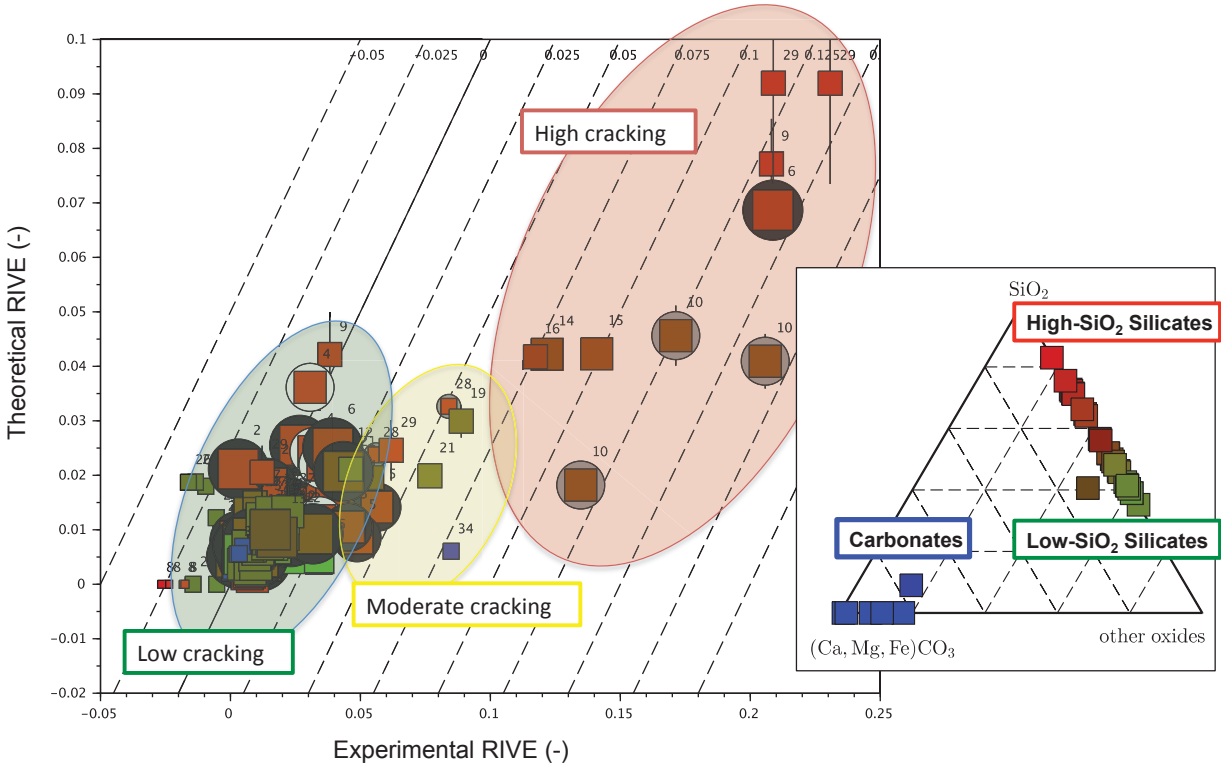

Figure 8. Estimation of post-irradiation cracking of varied aggregates. The theoretical RIVEs are derived from linear homogenization theory applied to uncracked polycrystallin materials (See equations in [Le Pape et al., 2016, Appendix A]). Each mark corresponds to the RIVE of a given aggregate at given fluence and irradiation conditions. The fill color is based of the oxide composition (ternary diagram): Red corresponds to high-silica content, blue to carbonate-rich minerals and, green to other-oxides-rich minerals (typically low-silica content). The size of the mark is proportional to the average grain size. The printed numbers located near each symbol correspond to the aggregate ID# in the IMAC database. Circles around square mark indicates the presence of micas: white for muscovite, black for biotite, or gray if unspecified.

6.2 YOUNG MODULUS

While RIVE data are plotted in Denisov et al.'s book, as a function of fluence and some indication on the average irradiation temperature, the loss of mechanical properties are not plotted as extensively. Partial data are tabulated and were introduced in the database. Other data could be reconstructed from the correlations between the plots showing the loss of mechanical properties against the aggregate expansion, and those presenting the expansions as a function of irradiation fluence and temperature. For the sake of illustration, Figure 9 presents the evolution of the relative Young modulus of irradiated aggregates (reference: unirradiated samples) with the radiation-induced volumetric expansion. Uncolored and colored marks correspond to the originally digitized data, and, correlation-based reconstructed data, respectively. Only 50% of the data could be recovered using this correlation analysis, i.e., associating a most likely fluence and irradiation temperature exposure to each Young modulus data. For most aggregates, the relative Young modulus exhibits a sharp decrease, here modeled by an exponential decay, with increasing RIVE. The limited data of the evolution of elastic properties of irradiated minerals (Mayer and Gigon [1956], Mayer and Lecomte [1960] and recent nano-indentation testing at ORNL) suggest that the observed losses are to be be attributed to cracking, judging by the severe degration of the Young modulus. Interestingly, such a trend is qualitatively similar to ASR-expansion-induced loss of modulus. In the sense of cracked homogeneous material [Budiansky and O'Connell, 1976], the loss of Young modulus can be almost directly interpreted as the increase of cracking density. Future analysis base on upscaling (homogenization) techniques should be able to assess the extent of irradiated-aggregate cracking.

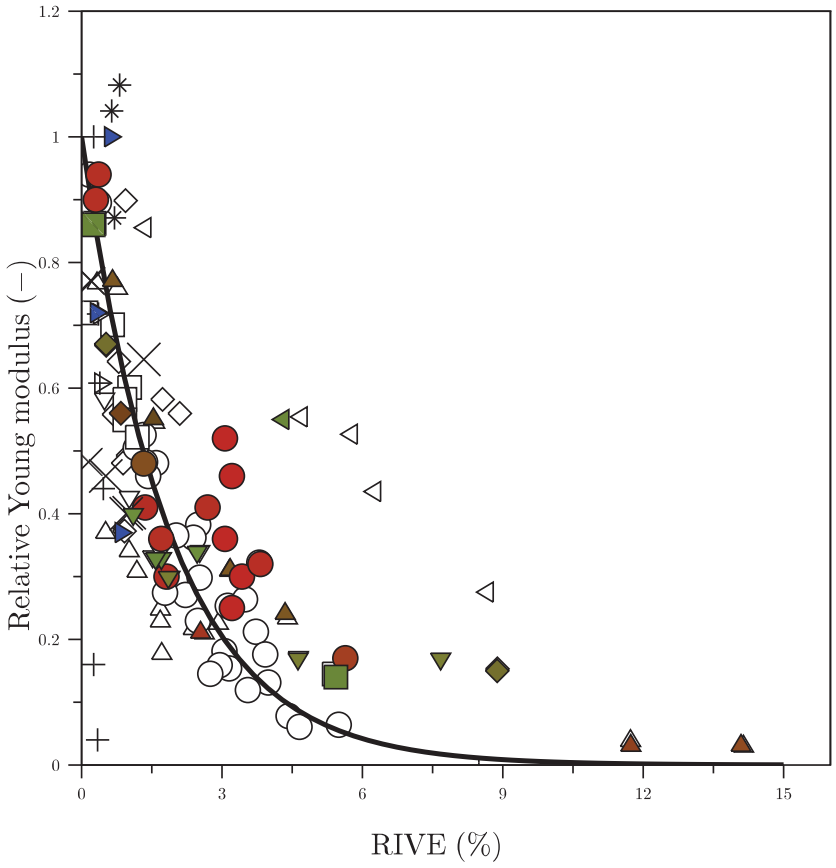

Figure 9. Irradiated aggregates: relative Young modulus as a function of RIVE. Hollow symbols: digitized data from [Denisov et al., 2012, Fig. 3.11] (92 data). Color-filled symbol: reconstructed data from the correlation of [Denisov et al., 2012, Fig. 3.11] and other expansion data [Denisov et al., 2012, Fig. 3.1.-3.4.], the RGB color chart is based on the silica content [SiO_2] (red), the carbonate content [$(Ca, Mg, Fe)CO_3$] (blue) and other oxide content (green). Solid line: exponential decay trend line, $\Delta E/E_0 \approx \exp(-0.528\varepsilon^*)$ with ε^* in (%). ($\triangle$): albitite, gabbro, labradorite, urtite; ($\triangleleft$): auleurolite; ($\diamond$): basalt, diabase; ($\circ$): granite, graniodorite, diorite, andesite; ($\square$): hornblendite; ($\times$): dolomite, limestone; ($\triangleright$): magnesite; ($\triangledown$): pyroxenite, peridotite, olivinite, dunite; ($*$): sandstone; ($+$): siderite.

7. FY2017-18 DEVELOPMENT SCHEDULE

IMAC v.0.1 – Minerals (December 2016): Released.

IMAC v.0.2 – Aggregate (April 2017): Released. IMAC v.0.3 – Concrete (August 2017): This document. An early database of irradiated concrete properties was created at ORNL [Field et al., 2015]. The development tasks consisted in: (1) creating a more advanced data structure to include additional properties and metadata, (2) transferring the previously acquired data in IMAC, and, (3) including addition data from the Russian literature.

IMAC v.1.0 – Restricted release (October 2017): This version of the database will be put on a server accessible to external users (i.e., non-ORNL). Access will require credentials provided by ORNL. It is envisioned to provide initial access to the ICIC members only to receive comments on possible improvements and bug fixes. Official announcement will be made at the Third General Meeting of the ICIC in Prague, November 6-10.

IMAC v.1.1 – public release (January 2018): This version of the database will be put on a publicly-accessible. Access will still require credentials provided by ORNL.
The interpretation of the collected data will continue during FY18 with the objectives of completing two additional reports:

1. The detailed analysis of irradiation-induced aggregate expansion and damage based on IMAC database (December 2017), and,
2. The detailed analysis of irradiation-induced concrete expansion and damage based on IMAC database (April 2018).

8. ACKNOWLEDGEMENTS

This material is based upon work supported by the U.S. Department of Energy, Office of Nuclear Energy, Light Water Reactor Sustainability Program, under contract number DE-AC05-00OR22725.
The development of this database was made possible thanks to the thorough literature search, digitization of data, and coding efforts of Mustafa Hameed Fayyadh Alsaid and Caleb Clement, respectively Master's Student at the University of Tennessee, and Undergraduate Student at the Tennessee Technological University.

References

ASTM C294-12. *Standard Descriptive Nomenclature for Constituents of Concrete Aggregates*. Committee C09, 100 Barr Harbor Drive, PO Box C700, West Conshohocken, PA 19428-2959, USA.

B. Budiansky and R. O'Connell. Elastic moduli of a cracked solid. *International Journal of Solids and Structures*, 12:81–97, 1976.

A. Chisolm Batten. Effect of irradiation on the strength of concrete. Technical report, Atomic Energy Research Establishment, Harwell, 1960. 13 p.

F. Clarke and H. Washington. The composition of the Earth crust. Technical report, United States Geological Survey, 1924.

H. J. Crawford and M. Wittels. Radiation stability of nonmetals and ceramics. In *Proceedings of the Second U.N. International Conference on the Peaceful Uses of Atomic Energy*, volume 5, pages 300–310, 1958.

W. Deer, R. Howie, and J. Zussman. *Rock forming minerals, Framework silicates*, volume Vol. 4. John Wiley, New York, 1963.

W. Deer, R. Howie, and J. Zussman. *Rock-forming minerals. Frameworks silicates: feldspars*, volume Volume 4A. The Geological Society, second edition edition, 2001.

W. Deer, R. Howie, and J. Zussman. *Rock forming minerals: Micas*, volume 3A. The Geological Society, London, 2003.

W. Deer, R. Howie, and J. Zussman. *Rock forming minerals: Non-silicates*, volume 5A. The Geological Society, London, 2011.

W. A. Deer, R. A. Howie, and J. Zussman. *Rock forming minerals: Orthosilicates*, volume 1A. The Geological Society, London, 1997a.

W. A. Deer, R. A. Howie, and J. Zussman. *Rock forming minerals: Single-chain silicates*, volume 2A. The Geological Society, London, 1997b.

W. A. Deer, R. A. Howie, and J. Zussman. *Rock forming minerals: Double-chain silicates*, volume 2B. The Geological Society, London, 1997c.

W. A. Deer, R. A. Howie, and J. Zussman. *Rock forming minerals, Framework Silicates*, volume 4B. The Geological Society, London, 2004.

W. A. Deer, R. A. Howie, and J. Zussman. *Rock forming minerals: Layered Silicates Excluding Micas and Clay Minerals*, volume 3B. The Geological Society, London, 2009.

A. Denisov, V. Dubrovskii, and V. Solovyov. *Radiation Resistance of Mineral and Polymer Construction Materials*. ZAO MEI Publishing House, 2012. in Russian.

J.-C. Dran, J.-C. Petit, T. Pro, J.-M. Lameille, and M. Montagne. Radiation enhanced solubility of calcite: implications for actinide retention. *Nuclear Instruments & Methods in Physics Research*, B65:330–334, 1992.

V. Dubrovskii, S. Ibragimov, M. Y. Kulakovskii, A. Y. Ladygin, and B. Pergamenshchik. Radiation damage in ordinary concrete. *Atomnaya Énergiya*, 23(4):310–316, October 1967.

V. Dubrovskii, S. IIbragimov, V. Korenevskii, A. Y. Ladygyn, V. Pergamenshchik, and V. Perevalov. Hematite concrete for shielding against high neutron fluxes. *Atomnaya Energiya*, 28(3):258–260, 1970a.

V. Dubrovskii, B. Pergamenshchik, V. Korenevskii, and V. Perevalov. Change of concrete aggregate properties under effect of neutron irradiation. *Concrete and Reinforced Concrete*, 9:25–27, 1970b. in Russian.

R. Eby, R. Ewing, and R. Birtcher. The amorphization of complex silicates by ion-beam irradiation. *Journal of Materials Research*, 7(11):3080–3102, 1992.

L. Elleuch, F. Dubois, and J. Rappeneau. Effects of neutron radiation on special concretes and their components. *Special Publication of The American Concrete Institute*, 43:1071–1108, 1972.

T. Esselman and P. Bruck. Expected condition of concrete at age 80 of reactor operation. Technical Report A13276-R-001, Lucius Pitkins, Inc., 36 Main Street, Amesbury, MA 01913, September 2013.

K. Field, I. Remec, and Y. Le Pape. Radiation effects on concrete for nuclear power plants – Part I: Quantification of radiation exposure and radiation effects. *Nuclear Engineering and Design*, 282:126–143, 2015.

B. Fournier and M. A. Bérubé. Alkali-aggregate reaction in concrete: a review of basic concepts and engineering implications. *Canadian Journal of Civil Engineering*, 27(2):167–191, 2000.

K. Fukuya, H. Nakata, K. Fujii, I. Kimura, M. Ohmura, H. Kitagawa, T. Itoh, and K. Shin. Radiation field analyses in reactor vessels of PWRs. *Institute of Nuclear Safety System Journal*, 9:153–161, 2002. URL `http://www.inss.co.jp/e/seikae/journal9e/j9_16e.htm`.

A. Giorla, M. Vaitová, Y. Le Pape, and P. Štemberk. Meso-scale modeling of irradiated concrete in test reactor. *Nuclear Engineering and Design*, 295:59–73, 2015.

A. Giorla, Y. Le Pape, and H. Huang. Meso-scale modeling of irradiation in pressurized water reactor concrete biological shield. In V. Saouma, J. Bolander, and E. Landis, editors, *Proceedings of FraMCoS-9*, Berkeley, CA, May-June 2016. IA-FraMCoS. doi: 10.21012/FC9.238. URL `http://www.framcos.org/FraMCoS-9.php#gsc.tab=0`.

A. Giorla, Y. Le Pape, and C. Dunant. Computing creep-damage interactions in irradiated concrete. *Journal of Nanomechanics and Micromechanics*, 04017001, 2017. Accepted.

B. Gray. The effects of reactor radiation on cement and concrete. In *Proceedings of an Information Exchange Meeting on 'Results of Concrete Irradiation Programmes'*, volume EUR 4751 f-e, Brussels, Belgium, April 19 1971. Commission des Communautés Européennes.

H. Hilsdorf, J. Kropp, and H. Koch. The effects of nuclear radiation on the mechanical properties of concrete. *Special Publication of The American Concrete Institute*, 55:223–254, 1978.

B. Kelly, J. Brocklehurst, D. Mottershead, and S. McNearney. The effects of reactor radiation on concrete. In *Proceedings of the Second Information Meeting on Pre Stress Concrete and Reactor Pressure Vessels and their Thermal Isolation*, volume EUR-4531, pages 237–265, Brussels, 1969.

G. Krivokoneva. Structural changes in feldspars under impact of radiation. *Crystal Chemistry and Structural Features of Minerals*, Leningrad, Nauka:75–79, 1976. (In Russian).

Y. Le Pape, K. Field, and I. Remec. Radiation effects in concrete for nuclear power plants – Part II: Perspective from micromechanical modeling. *Nuclear Engineering and Design*, 282:144–157, 2015.

Y. Le Pape, A. Giorla, and J. Sanahuja. Combined effects of temperature and irradiation on concrete damage. *Journal of Advanced Concrete Technology*, 14(3):70–86, 2016. doi: doi:10.3151/jact.14.70.

Y. Le Pape, M. Alsaid, and A. Giorla. Radiation-induced volumetric expansion of rock-forming minerals. *Journal of Nuclear Materials*, 2017. submitted.

K. Levenberg. A method for the solution of certain non-linear problems in least squares. *Quarterly of Applied Mathematics*, 2:164–168, 1944.

D. Marquardt. An algorithm for least-squares estimation of nonlinear parameters. *SIAM Journal on Applied Mathematics*, 11(2):431–441, 1963.

G. Mayer and J. Gigon. Effets des neutrons rapides sur quelques constantes physiques du quartz cristallin et de la silice vitreuse. *Le Journal de Physique et le Radium*, 18:109–114, 1956.

G. Mayer and M. Lecomte. Effet des neutrons rapides sur le quartz cristallin et la silice vitreuse. *Le Journal de Physique et le Radium*, 21(12):846–852, 1960.

S. Muto and I. Maruyama. Electron irradiation-induced density change of natural rock minerals, α-quartz, orthoclase, and muscovite. 70th Cement Technology Tournament Abstracts, 2016. 1317:120-121.

W. Primak. Fast-neutron-induced changes in quartz and vitreous silica. *Physical Review*, 110(6):1240–1254, 1958. ISSN 0031-899X.

F. Rajabipour, E. Giannini, C. Dunant, J. H. Ideker, and M. D. Thomas. Alkali-silica reaction: current understanding of the reaction mechanisms and the knowledge gaps. *Cement and Concrete Research*, 76: 130–146, 2015.

I. Remec, T. Rosseel, K. Field, and Y. Le Pape. Characterization of radiation fields for assessing concrete degradation in biological shields of NPPs. In *9th Topical Meeting of the Radiation Protection and Shielding Division of the American Nuclear Society – (RPSD-2016)*, Paris, France, October 3-6 2016.

T. Rosseel. Status report on the second single variable mineral analogue experiment. Technical Report ORNL/TM-2016/285, Oak Ridge National Laboratory, June 2016.

T. Rosseel, I. Maruyama, Y. Le Pape, O. Kontani, A. Giorla, I. Remec, J. Wall, M. Sircar, C. Andrade, and M. Ordonez. Review of the current state of knowledge on the effects of radiation on concrete. *Journal of Advanced Concrete Technology*, 14:368–383, 2016. Accepted.

J. Seeberger and H. Hilsdorf. Einfluß von radioactiver Strahlung auf die Festogkeit and Struktur von Beton. Technical Report NR 2505, Institut für Massivbau and Baustofftechnologie, Universität Karlsruhe, 1982.

K. Wedepohl. *Geochemistry*. Holt, Reinhart and Winston, 1971.

D. Whitney and B. Evans. Abbreviations for names of rock-forming minerals. *American Mineralogist*, 95: 185–187, 2010.

K. Willam, Y. Xi, and D. Naus. A review of the effects of radiation on microstructure and properties of concretes used in nuclear power plants. Technical Report NUREG/CR-7171 ORNL/TM-2013/263, U.S. Nuclear Regulatory Commission, Washington, DC 20555-0001, November 2013.

M. Wittels. Structural behavior of neutron irradiated quartz. *Philosophical Magazine*, 2:1445–1461, 1957.

C. Wong. Neutron radiation damage in some birefringent crystals. *Physics Letters A*, 50(5):346, 1974.

V. Zubov and A. Ivanov. Expansion of quartz caused by irradiation with fast neutrons. *Soviet Physics Crystallography*, 11(3):372–374, 1966.

V. Zubov and A. Ivanov. Elasticity of quartz irradiated with fast neutrons. *Soviet Physics Crystallography*, 12 (2):313–314, Sept.-Oct. 1967.

A APPENDIX A: AGGREGATES AND MINERALS HIERACHICAL CLASSIFICATION

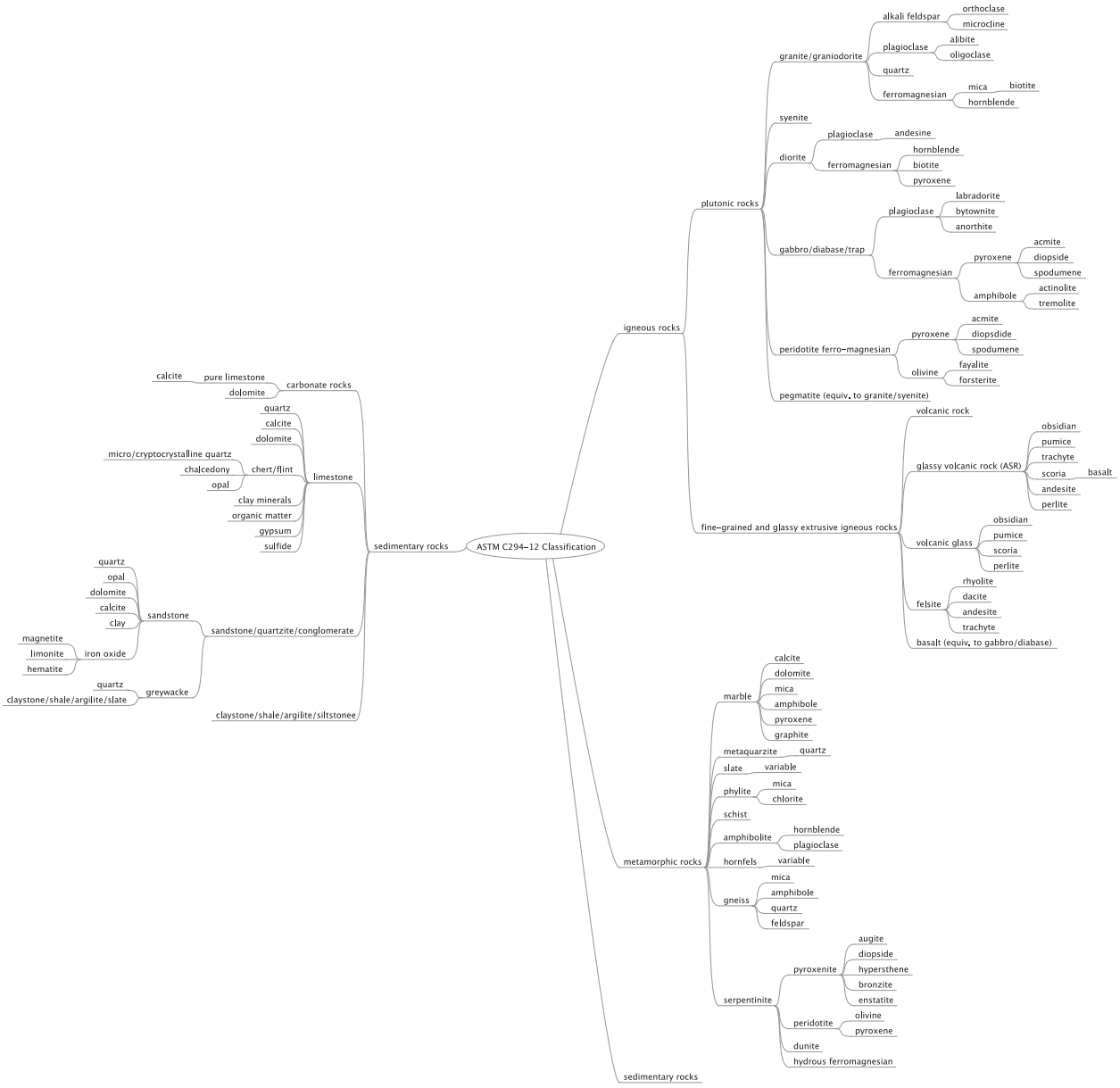

Figure 10. ASTM C294 hierarchical classification of aggregate used in concrete. The ramification extremities show the possible minerals constitutive of the rocks.

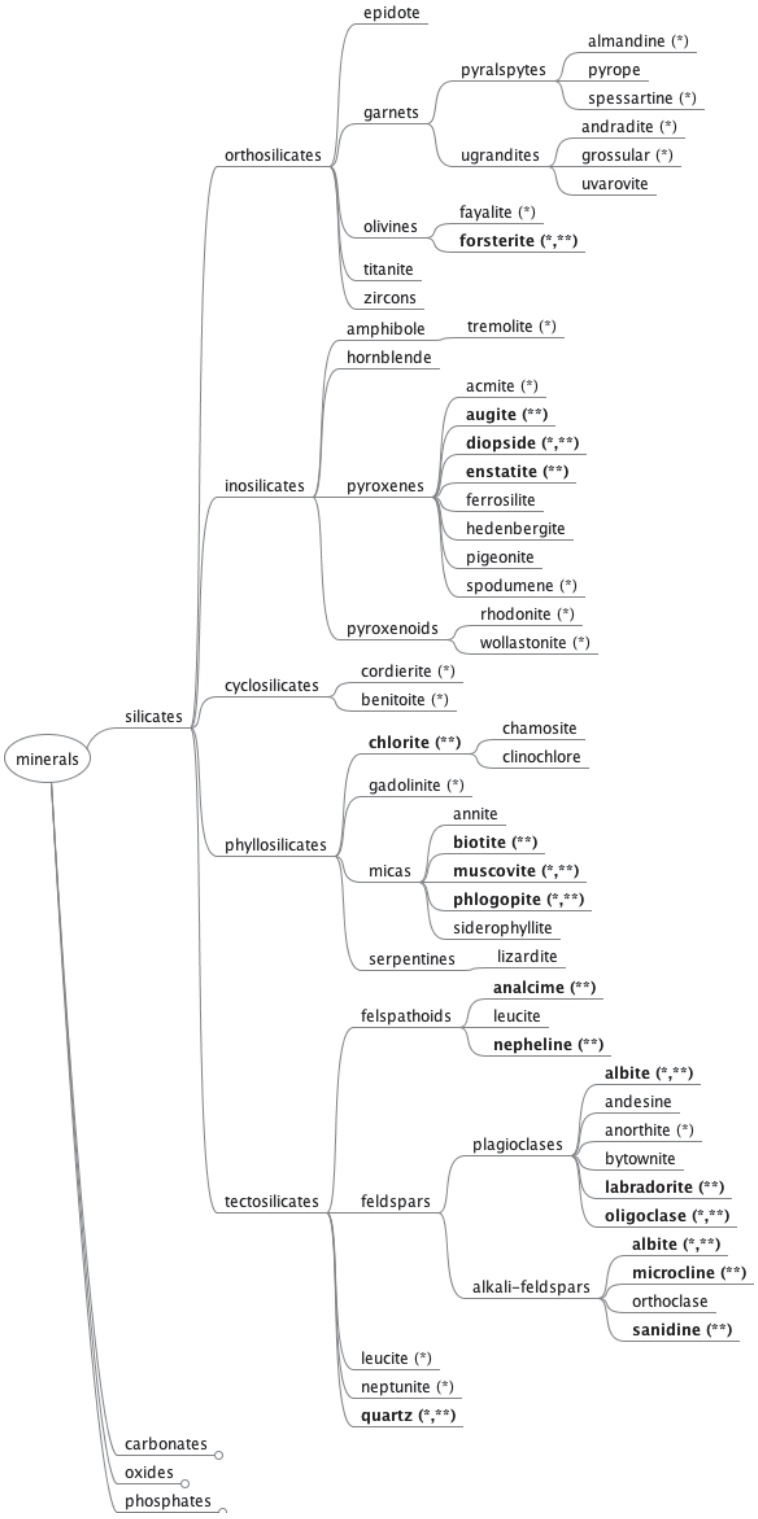

Figure 11. Hierarchical classification of silicates (non exhaustive list). (*) indicates available data obtained by ion-beam irradiation, i.e., critical amorphization dose; (**) corresponds to available data obtained by neutron irradiation.